2-Amino-4-nitroaniline, a Known Compound with Unexpected Properties

Tsonko Kolev,*,†,‡ Bojidarka B. Koleva,§ Michael Spiteller,|| Heike Mayer-Figge,⊥ and William S. Sheldrick⊥

Institute of Organic Chemistry, Bulgarian Academy of Sciences, Acad. G. Bonchev Str. build. 9, 1113 Sofia, Bulgaria, Department of Organic Chemistry, Faculty of Chemistry, Plovdiv University "P. Hilendarski", Plovdiv 4000, Bulgaria, Department of Analytical Chemistry, Faculty of Chemistry, Sofia University "St. Kl. Ohridsky", 1164 Sofia, Bulgaria, Institut für Umweltforschung, Universität Dortmund, Otto-Hahn-Strasse 6, 44221 Dortmund, Germany, and Lehrstuhl für Analytische Chemie, Ruhr-Universität Bochum, Universitätsstrasse 150, 44780 Bochum, Germany

Received: December 20, 2006; In Final Form: April 26, 2007

2-Amino-4-nitroaniline crystallizes in a noncentrosymmetric space group, which gives it significant potential for second-order nonlinear optical properties (NLO) in the bulk. Crystallographic and linear-polarized IR-spectrocopic data in the solid state unambiguously confirm a quinoide-like structure in the ground state in contrast to UV and theoretical data, which indicate an aromatic one for the excited state. UV−vis spectral elucidations in solutions with different polarities indicate a significant charge-transfer band with shifts of up to 100 nm, corresponding to a large value for the molecular first hyperpolarizability. Calculations of the UV- and IR-spectroscopic properties confirm the stabilization of the quinoide-like structure in the ground state, as well as the theoretically predicted NLO properties at the molecular level and provide a value of β_{tot}, which is some 3.6 times higher than the analogous parameter for *p*-nitroaniline, a classical compound with experimentally confirmed NLO properties.

1. Introduction

One of the most important tasks of molecular engineering is the efficiency−transparency tradeoff. Conjugated and polar molecules possessing the CT characteristics needed for large hyperpolarizability exhibit an almost inevitable loss of transparency. The optimization of molecular hyperpolarizability and the ability of such molecules to pack in the crystal in a useful fashion are also very important. The nonlinear optical properties (NLO) of organic molecules and crystals are of great interest in physics, chemistry, and applied technologies, with a view to expanding the application of organic materials in the field of nonlinear optics (NLO). It is well-known that 4-nitroanilines show NLO and electro-optical (EO) effects.[1] Their electronic nonlinearity is based on molecular units containing a strongly delocalized p-electron system, with donor ($-NH_2$) and acceptor ($-NO_2$) groups sited at opposite ends of the molecule.[2]

Interest in 2-amino-4-nitroaniline (**1**, Scheme 1) is based on its similarity to p-nitroaniline and a previous lack of spectroscopic and structural investigations. The properties of **1** have been studied by means of UV and linear polarized IR spectroscopy in the solid state as well as by single-crystal X-ray diffraction. The theoretical ab initio and DFT data support the experimental results as well as predicting its NLO properties.

2. Experimental Section

2.1. Materials. 2-Amino-4-nitroaniline was received from the Schuchard, Muenchen, Germany, as a red powder and was recrystallized three times, first from a water−ethanol (1:2) solvent mixture and then twice from 96% ethanol. Single prismatic crystals, suitable for X-ray analyses, were grown from methanol at room temperature over a period of 3 weeks. (Found: C, 47.05; H, 4.61; N, 27.45. $[C_6H_7N_3O_2]$ Calcd: C, 47.06; H, 4.61; N, 27.44%). The most intensive signal in the mass spectrum is that of the peak at 154.21 *m/z*, corresponding to the singly charged cation $[C_6H_8N_3O_2]^+$ with a molecular weight of 154.15.

SCHEME 1: Chemical Structure of 2-Amino-4-nitroaniline (1) and Its Quinoide Form (2)

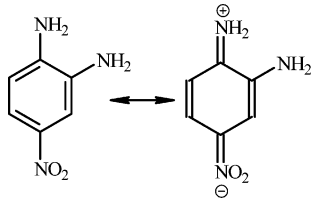

(**1**) (**2**)

2.2. Methods. ***2.2.1. X-ray Diffraction.*** The X-ray diffraction intensities were measured in the ω scan mode on a Siemens *P*4 diffractometer equipped with Mo Kα radiation ($\lambda = 0.710\,73$ Å, $\theta_{max} = 25°$). The structure was solved by direct methods and refined against F^2.[3,4] Figure 1 illustrates the anion and cation structures with thermal ellipsoids being depicted at the 50% probability level. Relevant crystallographic structure data and refinement details are presented in Table 1, and selected bond distances and angles are given in Table 2. The hydrogen atoms were constrained to calculated positions and refined using riding models in all cases. As there are no atom types heavier than oxygen in the structure, the absolute structure could not be determined with certainty using Mo K radiation.

* Corresponding author. Tel.: (3592) 9606 106. E-mail: kolev@orgchm.bas.bg.
† Bulgarian Academy of Sciences.
‡ Plovdiv University "P. Hilendarski".
§ Sofia University "St. Kl. Ohridsky".
|| Universität Dortmund.
⊥ Ruhr-Universität Bochum.

10.1021/jp068761x CCC: $37.00
Published on Web 09/15/2007

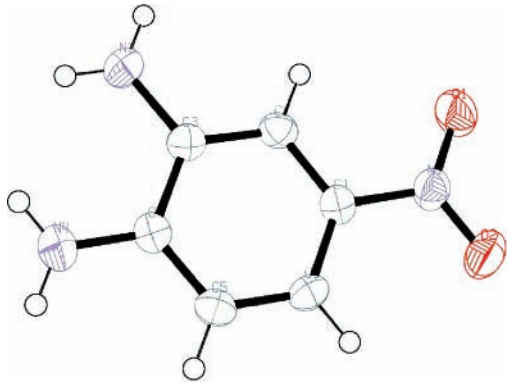

Figure 1. ORTEP plot of **1** with 50% thermal ellipsoids; hydrogen atoms are shown as spheres of arbitrary radii.

TABLE 1: Crystal Data, Data Collection, and Refinement Conditions for $C_6H_7N_3O_2$

empirical formula	$C_6H_7N_3O_2$
formula weight	153.15
temperature	293(2) K
wavelength	0.71073 Å
crystal system	orthorhombic
space group	*P*2(1)2(1)2(1)
unit cell dimensions	$a = 3.7590(8)$ Å
	$b = 10.307(2)$ Å
	$c = 17.290(4)$ Å
	$\alpha = \beta = \Gamma = 90°$
volume	669.9(2) Å^3
Z	4
calculated density	1.519
absorption coefficient	0.118
F(000)	320
crystal size	0.43 × 0.36 × 0.28 mm
θ range for data collection	7.50−15.00°
limiting indices	$0 \Leftarrow h \Leftarrow 4$
	$0 \Leftarrow k \Leftarrow 12$
	$0 \Leftarrow l \Leftarrow 20$
absorption correction	0.118
refinement method	full-matrix least-squares on F^2
goodness-of-fit on F^2	1.070
final *R* indices [$I > 2\sigma(I)$]	$R1 = 0.0388$, $wR2 = 0.1037$
R indices (all data)	$R1 = 0.0471$, $wR2 = 0.1085$

TABLE 2: Selected Bond Lengths (Å) and Angles (deg) for $C_6H_7N_3O_2$[a]

C1−C6	1.387(4)	C6−C1−C2	121.8(2)
C1−C2	1.397(4)	C6−C1−N1	119.2(2)
C1−N1	1.441(3)	C2−C1−N1	119.0(2)
N1−O1	1.238(3)	O1−N1−O2	121.9(2)
N1−O2	1.246(3)	O1−N1−C1	119.3(2)
C2−C3	1.379(4)	O2−N1−C1	118.8(2)
C3−N3	1.422(4)	C3−C2−C1	120.0(2)
C3−C4	1.427(4)	C2−C3−N3	121.1(2)
C4−N4	1.367(4)	C2−C3−C4	119.1(2)
C4−C5	1.405(4)	N3−C3−C4	119.7(2)
C5−C6	1.383(4)	N4−C4−C5	120.2(3)
		N4−C4−C3	120.4(3)
		C5−C4−C3	119.5(2)
		C6−C5−C4	120.8(3)
		C5−C6−C1	118.8(3)

[a] Symmetry transformations used to generate equivalent atoms: #1 $-x, -y + 1, -z + 1$.

2.2.2. Conventional and Polarized IR Spectroscopy. The IR spectra were measured on a Thermo Nicolet OMNIC FTIR spectrometer (4000−400 cm^{-1}, 2 cm^{-1} resolution, 200 scans) equipped with a Specac wire-grid polarizer. Nonpolarized solid-state IR spectra were recorded using the KBr disk technique. The oriented samples were obtained as a suspension in a nematic liquid crystal (MLC 6815, Merck) with the presence of an isolated nitrile stretching IR band at about 2245 cm^{-1} additionally serving as an orientation indicator. The theoretical approach and the experimental technique for preparing the samples have been previously presented, as have procedures for the interpretation of polarized IR spectra. The validation of this novel linear-dichroic infrared (IR-LD) orientation solid-state method with regard to accuracy, precision, and the influence of the liquid crystal medium on peak positions and integral absorbance of the guest molecule bands has also been reported.[5−7]

Optimization strategies for the experimental conditions and an experimental design for the quantitative evaluation of the impact of four input factors have been presented.[6,7] The necessary number of scans, the rubbing-out procedures for KBr pellets, the required sample quantities for the liquid crystal medium, and the optimum ratios of Lorentzian to Gaussian peak functions in the curve fitting procedure for the spectroscopic signal at five different frequencies have all been investigated.[6,7] It has been established that the procedure for the determination of the position (ν_i) and integral absorbance (A_i) for each *i*-peak can be carried out by deconvolution and curve-fitting at a 50:50% ratio of Lorentzian to Gaussian peak functions, for χ^2 factors within 0.00066−0.00019 (in our case) and 2000 iterations.[6,7] The means of two such treatments were compared by the Student *t*-test. The experimental IR-spectral patterns were acquired and processed by GRAMS /AI 7.01 IR spectroscopy (Thermo Galactic) and STATISTICA for Windows 5.0 (StatSoft, Inc., Tulsa, OK) program packages. The applicability of the latter approach to experimental IR-spectroscopic band assignment as well as in obtaining stereo-structural information has been demonstrated for a series of organic systems and coordination complexes of heterocyclic ligands, including codeine derivatives, Cu(II) complexes, and their polymorphs, as well as Au(III) peptide complexes and their hydrochlorides and hydrogensquarates. The theory of IR-LD spectroscopy and the employed polarized IR-spectra interpretation difference-reduction procedure are given in references.[8−21]

2.2.3. Mass Spectral Data. The FAB mass spectra were recorded on a Fisons VG Autospec instrument employing 3-nitrobenzylalcohol as the matrix.

2.2.4. UV Spectra. UV spectra were recorded using 0.0921 cm quarz cells on a Tecan Safire Absorbance/Fluorescence XFluor 4 V 4.40 spectrophotometer operating between 190 and 900 nm, and employing water, methanol, dichloromethane, tetrahydrofuran, acetonitrile, acetone, 2-propanol, and ethyl acetate (all Uvasol, Merck products) as solvents at a concentration of 2.5×10^{-5} M.

2.2.5. Quantum Chemical Calculations. These are were performed with the Gaussian 98 and Dalton 2.0 program packages.[22,23] The output files were visualized by means of the ChemCraft program.[24] The procedures and approaches are described in the following section.

The geometry of **1** was optimized at two levels of theory, namely by second-order Moller−Pleset perturbation theory (MP2) and by density functional theory (DFT) using the 6-311++G** basis set. The DFT method employed is B3LYP, which combines Backe's three-parameter nonlocal exchange function with the correlation functional of Lee, Yang, and Parr.[25,26] Molecular geometries of the studied species were fully optimized by the force gradient method using Bernys' algorithm.[27] For every structure, the stationary points found on the molecule potential energy hypersurfaces were characterized using standard analytical harmonic vibrational analysis. The absence of the imaginary frequencies, as well as of negative eigenvalues of the second-derivative matrix, confirmed that the

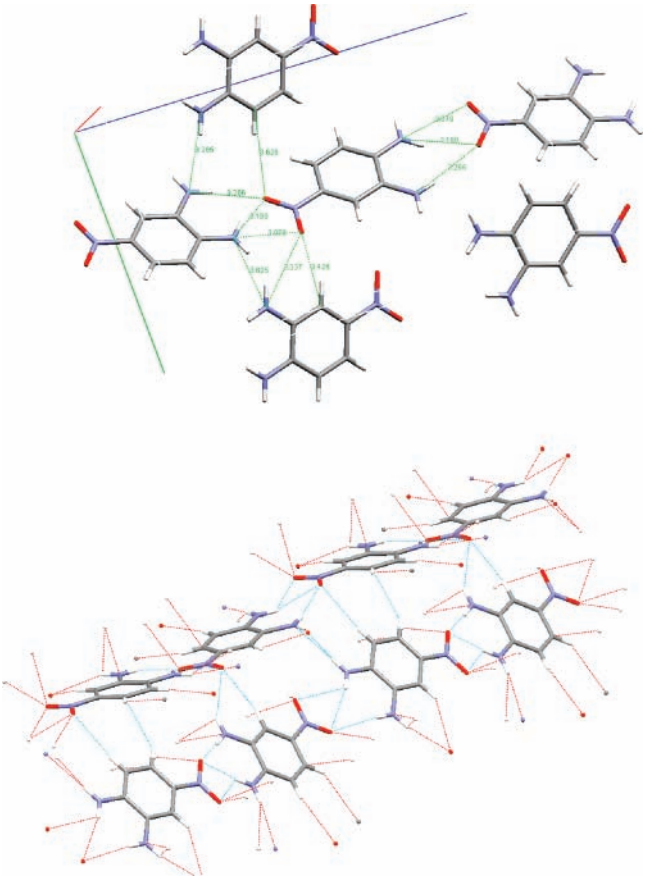

Figure 2. Extended unit cell and short contacts in the structure of **1**.

stationary points correspond to minima of the potential energy hypersurfaces. The calculations of vibrational frequencies and infrared intensities were checked to establish which kind of performed calculations agreed best with the experimental data. In the case of **1**, the DFT method provides more accurate vibrational data, as far as the calculated standard deviations of respectively 10 (B3LYP) and 19 cm^{-1} (MP2) are concerned, which correspond to those groups not involved in intra- or intermolecular interactions. So, the B3LYP/6-311++G** data are presented for these modes, where a modification of the results using the empirical scaling factor 0.9614[28,29] was made to achieve a better correspondence between the experimental and theoretical values. The UV spectra of **1** in the gas phase and in ethyl acetate solution were obtained by CIS/6-311++G** and TDDFT calculations.

2.2.6. Thermal Analysis. The thermal analyses were performed in the temperature range 25−300 °C by employing a differential scanning calorimeter Perkin-Elmer DSC-7 and a differential thermal analyzer DTA/TG (Seiko Instrument, model TG/DTA 300). The experiments were carried out at a scanning rate of 10K/min under an argon atmosphere.

2.2.7. Elemental Analysis. The elemental analysis was carried out according to the standard procedures for C and H (as CO_2, and H_2O) and N (by the Dumas method).

3. Results and Discussion

3.1. Crystal and Electronic Structure. The studied compound crystallizes in the chiral noncentrosymmetric orthorhombic space group $P2_12_12_1$, a fact that should determine its NLO properties in the bulk. The asymmetric unit of **1** is shown in Figure 1, and a view of the structure perpendicular to [100] is given in Figure 2. Infinite layers of molecules are linked into a

SCHEME 2: Optimized Geometry of 1 in the Ground State

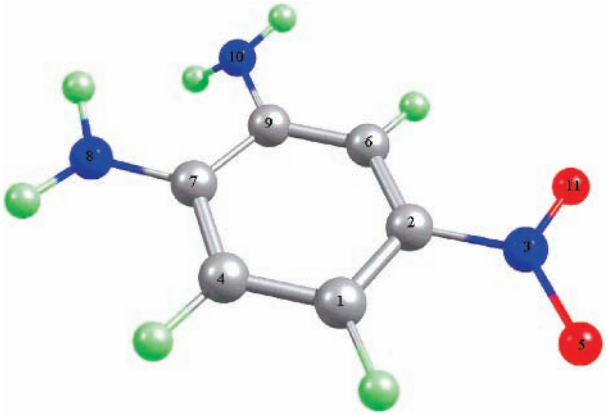

3D network by intermolecular contacts of the types $NH_2\cdots ONO$ (lengths: 2.573, 2.343, 2.581, 2.345, 3.266 Å), $CH\cdots ONO$ (2.619 Å), and $NH_2\cdots NH_2$ (2.413 Å) (Figure 2). The bond lengths and angles (Table 2) in the aromatic ring can be analyzed to establish whether they are more typical for a push−pull system or for a quinoide-like structure (Scheme 1). The C−C bond lengths in the aromatic ring are, in fact, characteristic for the latter structural type, as is the C4−N4 distance of 1.367 Å for the *p*-amino substituent. A much longer distance of 1.422 Å is observed for the C3−N3 bond of the *m*-amino substituent. The molecule is effectively flat with a deviation from total planarity of only 2.2°. The theoretically optimized geometry parameters for the molecule (Scheme 2) also indicate a near to bipolar structure (quinoide-like) in the ground state and a near to aromatic one in the excited state. The calculated dihedral angles and bond lengths for the MP2 method deviate in the first case from the experimental crystallographic values by less than 0.056 Å and 0.2°. The aromatic character in the excited state leads to a distortion from total planarity for the molecule, with both its NH_2 groups being tilted by dihedral angles of 14.0-(2)°, values that are typical for aromatic systems. The influence of the geometry employed for the calculation is identical for both methods, but the values obtained for the optimized dimensions with B3LYP/6-311++G** were greater than those others for the MP2/6-311++G** geometry by a factor of about 1.01 and the values for the latter level of theory correlated better with the crystallographic data (compare Tables 2 and 3). The lack of a second-order susceptibility for **1**, in contrast to centrosymmetric *p*-nitroaniline, is an expected property due to the noncentrosymmetric arrangement of its molecules in the crystal lattice

3.2. IR Spectra. The quinoide-like structure in the solid state is also confirmed spectroscopically by the linear-polarized IR data discussed below. A complete assignment of the IR bands of **1** to the corresponding normal vibrations was carried out by theoretical vibrational analysis.

The main differences between the calculated (Figure 3) and experimentally observed peak positions (Figure 4(1)) are associated with the stretching and bending modes of the NH_2 groups, as well as with those of the NO_2 one. The *p*-NH_2 group is characterized by a broad maximum at 3100−3000 cm^{-1}, which is typical for a positively charged group and belongs to the $\nu^{as}_{N\delta+H_2}$ and $\nu^{s}_{N\delta+H_2}$ modes. On the other hand, the scissoring $\delta_{N\delta+H_2}$ band also exhibits an unusual high-frequency shift (Figure 4(1)) to 1664 cm^{-1}, an observation that is in support of the presumption concerning partial charge redistribution. An opposite tendency is observed for the characteristic maxima of

TABLE 3: Selected Optimized Geometry Parameters of (1) in the Ground State at the MP2 Level of Theory and for the 6-311++G Basis Set Using the Atom Numbering in Scheme 2**

bond length (Å)		angle (deg)		dihedral angle (deg)	
R(1,2)	1.395	*A*(2,1,4)	118.9(5)	*D*(4,1,2,3)	179.3
R(1,4	1.389	*A*(1,2,3)	119.5(8)	*D*(4,1,2,6)	1.9
R(2,3)	1.447	*A*(1,2,6)	121.3(4)	*D*(2,1,4,7)	0.2
R(2,6)	1.400	*A*(3,2,6)	119.0(4)	*D*(12,1,4,7)	178.8
R(3,5)	1.272	*A*(2,3,5)	118.6(0)	*D*(1,2,3,5)	0.7
R(4,7)	1.406	*A*(2,3,11)	118.4(4)	*D*(1,2,3,11)	179.3
R(6,9)	1.387	*A*(5,3,11)	122.9(4)	*D*(6,2,3,5)	178.1
R(7,8)	1.379	*A*(1,4,7)	120.9(4)	*D*(6,2,3,11)	1.8
R(7,9)	1.426	*A*(2,6,9)	119.9(1)	*D*(1,2,6,9)	1.6
R(9,10)	1.411	*A*(4,7,8)	122.4(2)	*D*(3,2,6,9)	179.6
		A(4,7,9)	119.2(9)	*D*(1,4,7,8)	177.8
		A(8,7,9)	118.2(8)	*D*(1,4,7,9)	2.5
		A(6,9,7)	119.4(5)	*D*(2,6,9,7)	0.7
		A(6,9,10)	122.9(3)	*D*(2,6,9,10)	179.0
				D(4,7,9,6)	2.8
				D(4,7,9,10)	178.8
				D(8,7,9,6)	177.5
				D(8,7,9,10)	0.7

the NO_2 group, which is in accordance with a degree of push−pull (bipolar) structural character for **1** in ground state. The characteristic maxima for the skeletal in-plane and out-of-plane modes of the aromatic system are influenced to an insignificant degree and the differences between their theoretical and experimental positions all fall within the range 11−19 cm^{-1}. The stabilization of a push−pull type of structure also affects the characteristics of 1,2,4-tetrasubstituted benzene rings, where the typical 8a, 19a, 8b, and 19b modes as well as 11g and 4g are influenced and are not observed at their typical values of 1580 ± 25, 1475 ± 25, 1575 ± 25, 1410 ± 50, 880 ± 40, and 720 ± 50 cm^{-1}.[30] In 2-amino-4-nitroaniline, these modes exhibit the characteristics of conjugated double bonds with typical IR bands within the ranges 1640−1595 cm^{-1} ($\nu_{C=C}$) and 960−840 cm^{-1} ($\gamma_{=CH}$), respectively.[30]

The difference IR-LD spectrum of **1** in the solid state indicates a significant degree of macro-orientation of the crystalline compound with a difference between the positive and negative bands $\Delta I\nu I$ of 0.456.[6,7] Elimination of the 1641 cm^{-1} peak leads to disappearance of the broad maximum at 3100−3000 cm^{-1}, which assigns the peak as δ_{NH_2} of the *p*-NH_2 group. At the same time, the peak at 1290 cm^{-1} is eliminated, which is once again in accordance with the assumption of a push−pull like system (Scheme 1(**2**)), where the charge redistribution leads to planarity of the *p*-NH_2 group and a collinear disposition of $\nu^{s}_{NH_2}$, δ_{NH_2}, and $\nu^{s}_{NO_2}$ due to the last peak belonging to the stretching mode (Scheme 3). The procedure generates the maxima at 3432 cm^{-1} ($\nu^{as}_{NH_2}$) and at 3380 and 3328 cm^{-1} ($\nu^{s}_{NH_2}$), as well as that at 1664 cm^{-1} belonging to the second NH_2 group. The $\nu^{s}_{NH_2}$ band

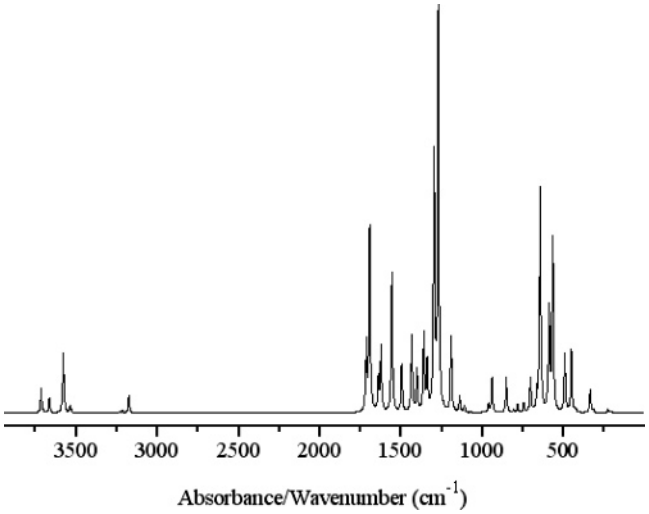

Figure 3. Calculated (nonscaled) IR spectrum of **1**.

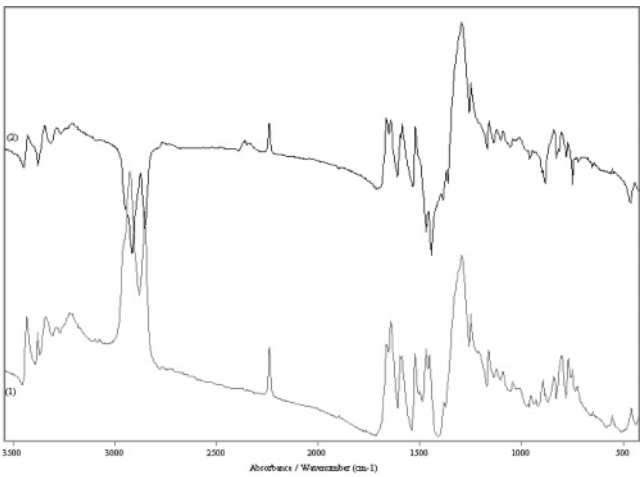

Figure 4. Nonpolarized IR (1) and difference IR-LD (2) spectra of **1**.

exhibits Fermi resonance and is split due to the participation of this group in asymmetric intermolecular H-bonds (see above). The high-frequency shift of the latter maximum can be attributed to this state of affairs. Elimination of the 1629 cm^{-1} peak causes a strong reduction of the a′ maxima at about 1600 cm^{-1} and in all peaks above 3000 cm^{-1}. This observation suggests that the 1629 cm^{-1} peak must belong to a partial CN double bond formed as a result of the push−pull system in the ground state. The transition moment of this peak is collinear to a pseudo a′ maxima and the elimination of the stretching peaks of both NH_2 groups is due to the mutual orientation of the molecules of **1** in the unit cell, resulting in a macro alignment of the discussed moments. The elimination of the 952 cm^{-1} peak (Figure 5(2))

SCHEME : 3 Visualization of Transition Moments of δ_{NH_2} (A), ν_{CN} (B), and $\nu^{s}_{NO_2}$ (C), Illustrating Their Mutual Collinearity in the Unit Cell of Molecule 1

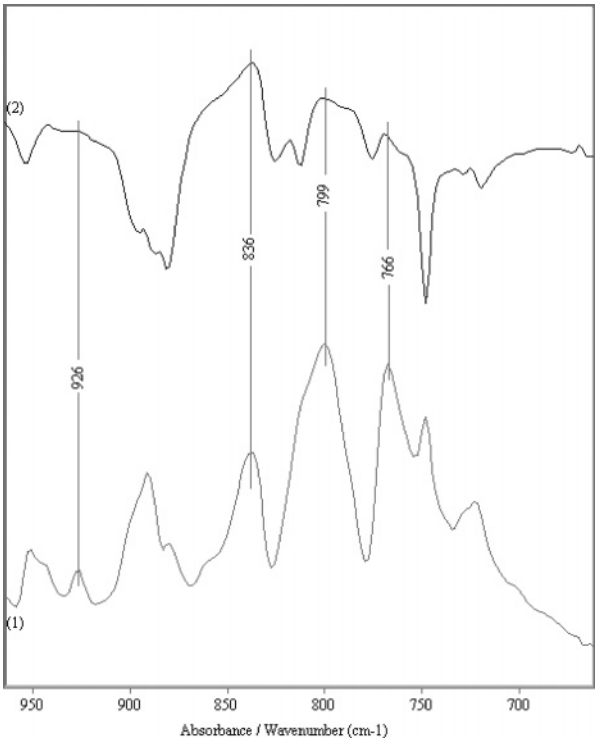

Figure 5. Nonpolarized IR (1) and reduced IR-LD (2) spectra of **1** after elimination of the peak at 926 cm^{-1}.

SCHEME 4: Planes of the Aromatic Systems in the Unit Cell of 1

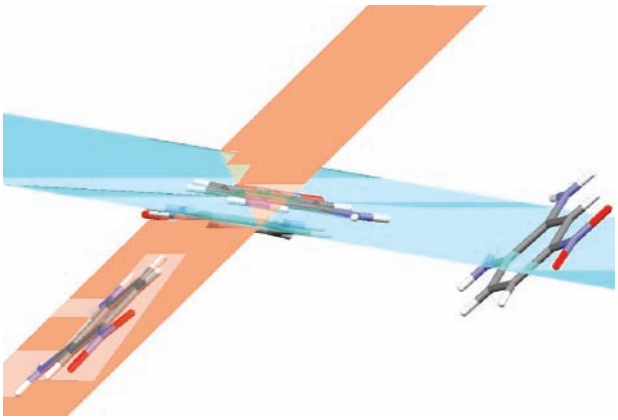

leads to disappearance of peaks at 904, 879, and 748 cm^{-1} peaks, all of which are assigned to the same symmetry class, being a″ out-of-plane modes as far as the asymmetric trisubstituted benzene belongs to the C_s point group. The experimental peak positions correspond well with the theoretically calculated values with deviations of less than 9 cm^{-1}. This data reduction led to the observation of second pairs of maxima belonging to same symmetry class (Figure 5(2)), due to the four molecules (**1**) in the unit cell being oriented as pairs at an angle of 54.2-(9)° (Scheme 4).

3.3. UV Spectra. The crystallographically determined noncentrosymmetric space group and the quinoide-like structure of **1** in the solid state prompted an investigation of its corresponding properties in solution.

The theoretically predicted electronic spectrum of **1** exhibits three bands at 191, 240, and 362 nm corresponding to K and B aromatic bands and a charge transfer (CT) transition. The calculated electronic properties are in good accordance with the experimentally observed UV spectra of **1** in different solvents,

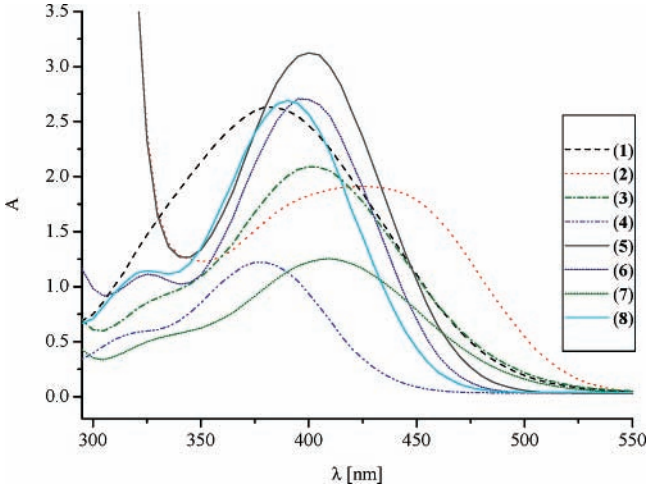

Figure 6. UV−vis spectra of **1** in H_2O (1), CH_3CN (2), CH_3OH (3), CH_2Cl_2 (4), $O{=}C(CH_3)_2$ (5), tetrahydrofuran (6), 2-propanol (7), and ethyl acetate (8).

as presented in Figure 6. On changing of the solvent from nonpolar CH_2Cl_2 to polar aprotic CH_3CN, a bathochromic shift of more than 100 nm is observed for the long wavelength CT band maximum. On the other hand, the band position in water is similar to that in CH_3Cl. It may be assumed that a positive or negative solvatochromism cannot be clearly defined for this compound, a fact that may be explained by the C_s symmetry of **1** in contrast to that of C_{2v} for *p*-nitroaniline, where a clear solvatochromism is apparent. In the case of 2-amino-4-nitroaniline, specific solvate interactions determine the presented results, but the observed significant value for its solvatochromism determines the NLO properties of **1** in solution as well.

3.4. Calculated NLO Properties of 1. The ground-state dipole moment of **1** calculated with the electron correlation method (B3LYP) is 8.2310 Debye. Compared to the value for *p*-nitroaniline[31−33] as the reference molecule, the lowering of this parameter by a factor of 3 for **1** can be explained by the presence of a second NH_2 group at the 2-position. This leads to a charge redistribution in the ground state and suggests that variations in the substitution pattern could be used to exploit the NLO properties of such pseudo C_s chromophores. The calculated single charges of the NH_2 and NO_2 groups in p-position in are −3.57 and +2.66 in the ground state. The second NH_2 group is also positively charged with a value of +0.07. The excited state exhibits respective values of −2.67, −0.98 and −0.74 eV for these groups. The calculated quadrupole moments in Debye Å ($XX = -68.14_4$, $YY = -55.09_1$, $ZZ = -66.19_7$, $XY = 1.00_3$, $XZ = 0.37_5$, $YZ = 1.69_3$) and octapole moments in Debye $Å^2$ ($XXX = 108.98_9$, $YYY = 8.15_4$, $ZZZ = 0.18_4$, $XYY = 28.19_0$, $XXY = -7.31_7$, $XXZ = 0.04_4$, $XZZ = -9.22_9$, $YZZ = 3.98_6$, $YYZ = 1.57_9$, $XYZ = 5.78_2$) exhibit values that are more than 3.6 times larger that the corresponding parameters for *p*-nitroaniline,[31−33] independent of the differing symmetries of the molecules. The calculated hexadecapole moments (Debye $Å^3$) also displays higher values than the reference material of $XXXX = -1689.97_7$, $YYYY = -492.82_9$, $ZZZZ = -68.92_5$, $XXXY = -25.99_4$, $XXXZ = -10.02_2$, $YYYX = 18.71_2$, $YYYZ = 0.95_4$, $ZZZX = 2.06_6$, $ZZZY = 1.77_8$, $XXYY = -355.59_0$, $XXZZ = -295.10_0$, $YYZZ = -116.92_6$, $XXYZ = 23.62_6$, $YYXZ = 6.85_8$, and $ZZXY = 3.32_4$, respectively.

3.5. TGV and DSC Data. TGV and DSC data are presented in Figure 7. The results clearly indicated an absence of any

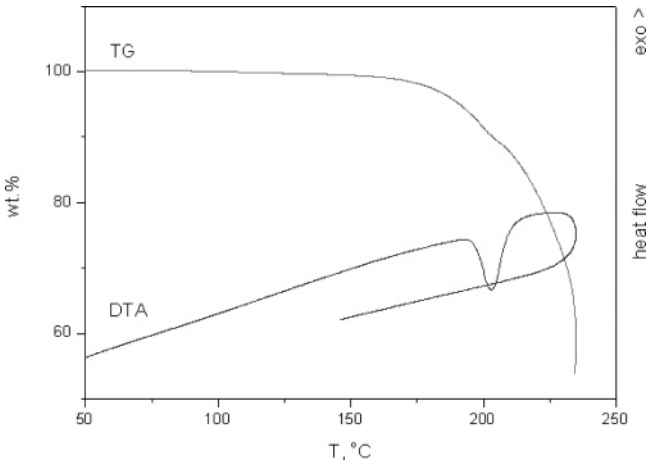

Figure 7. TGV and DSC data of **1** in the range 25−300 °C.

additional thermal transitions except for the sample melting in the temperature range 220.04 ± 0.5 °C, thus confirming the purity of the compound and its relevant stability up to its melting point.

4. Conclusions

A noncentrocymmetric crystal structure has been established for 2-amino-4-nitroaniline, which gives it a significant potential for second-order NLO properties in the bulk. Crystallographic and linear-polarized IR-spectrocopic data in the solid state unambiguously confirm a quinoide-like structure for the compound in the ground state. The UV−vis spectral elucidationin solutions with different polarities indicate a significant charge transfer (CT) band shifting of up to 100 nm, corresponding to a large molecular first hyperpolarizability value. The calculated NLO and UV- and IR-spectroscopic properties all confirm the latter assumption. The obtained value of $\beta_{tot.}$ is some 3.6 times higher than the value for *p*-nitroaniline. The large β value of the 2-amino-4-nitroaniline make this planar pseudo 1-D chromophore a very promising candidate for second-order NLO applications. It presents a simple compound but possesses a novel structural motif for designing NLO-active molecules with greater optical transparency in the bulk as well as in solution.

Acknowledgment. T.K., B.K., and M.S. thank the DAAD for a grant within the priority program "Stability Pact South-Eastern Europe" and the Alexander von Humboldt Foundation.

Supporting Information Available: Crystal data in CIF format. This material is available free of charge via the Internet at http://pubs.acs.org.[34]

References and Notes

(1) Chemla, D.; Zyss, J. *Nonlinear Optical Properties of Organic Molecules and Crystals*; Chemla. D., Zyss, J., Eds.; Academic Press: New York, 1987; Vol. 1, pp 23−187.

(2) Nalwa, H. S.; Watanabe, T.; Miyata, S. *Nonlinear Optics of Organic Molecules and Polymers*; Nalwa, H. S., Miyata, S., Eds.; CRC Press: Boca Raton, FL, 1997, pp 89−329.

(3) Sheldrick, G. M. SHELXTL, release 5.03, for Siemens R3 crystallographic research system; Siemens Analytical X-Ray Instruments, Inc.: Madison, WI, 1995.

(4) Sheldrick, G. M. SHELXS97 and SHELXL97. University of Goettingen, Germany, 1997.

(5) Ivanova, B. B.; Arnaudov, M. G.; Bontchev, P. R. *Spectrochim. Acta Part A* **2004**, *60* (4), 855.

(6) Ivanova, B. B.; Tsalev, D. L.; Arnaudov, M. G. *Talanta* **2006**, *69*, 822.

(7) Ivanova, B. B.; Simeonov, V. D.; Arnaudov, M. G.; Tsalev, D. L. *Spectrochim Acta Part A*, in press.

(8) Ivanova, B. B. *J. Mol. Struct*. **2005**, *738*, 233.

(9) Koleva, B. B. *J. Mol. Struct*., in press.

(10) Ivanova, B. B. *Centrl. Eur. J. Chem*. **2006**, *4*, 111.

(11) Koleva, B. B. *Vibr. Spectrosc*., in press.

(12) Ivanova, B. B. *J. Coord. Chem*. **2005**, *58* (7), 587.

(13) Bakalska, R.; Ivanova, B. B.; Kolev, Ts. *Centrl. Eur. J. Chem.* **2006**, *4* (3), 533.

(14) Ivanova, B. B. *J. Mol. Struct*. **2006**, *782*, 122.

(15) Ivanova, B. B. *Spectrochim. Acta* **2006**, *64A*, 931.

(16) Ivanova, B. B.; Kolev, T.; Zareva, S. Y. *Biopolymers* **2006**, *82*, 587.

(17) Koleva, B. B.; Kolev, Ts.; Zareva, S. Y.; Spiteller, M. *J. Mol. Struct*., in press.

(18) Koleva, B. B. *Spectrochim. Acta, Part A*, in press.

(19) Kolev, Ts.; Zareva, S. Y.; Koleva, B. B.; Spiteller, M. *Inorg. Chim. Acta*, in press.

(20) Koleva, B. B.; Kolev, Ts. M.; Spiteller, M. *Biopolymers*, in press.

(21) Kolev, Ts. *Biopolymers* **2006**, *83*, 39.

(22) Frisch, M. J.; Trucks, G. W.; Schlegel, H. B.; Scuseria, G. E.; Robb, M. A.; Cheeseman, J. R.; Zakrzewski, V. G.; Montgomery, J. A., Jr.; Stratmann, R. E.; Burant, J. C.; Dapprich, S.; Millam, J. M.; Daniels, A. D.; Kudin, K. N.; Strain, M. C.; Farkas, Ö.; Tomasi, J.; Barone, V.; Cossi, M.; Cammi, R.; Mennucci, B.; Pomelli, C.; Adamo, C.; Clifford, S.; Ochterski, J.; Petersson, G. A.; Ayala, P. Y.; Cui, Q.; Morokuma, K.; Salvador, P.; Dannenberg, J. J.; Malick, D. K.; Rabuck, A. D.; Raghavachari, K.; Foresman, J. B.; Cioslowski, J.; Ortiz, J. V.; Baboul, A. G.; Stefanov, B. B.; Liu, G.; Liashenko, A.; Piskorz, P.; Komáromi, I.; Gomperts, R.; Martin, R. L.; Fox, D. J.; Keith, T.; Al-Laham, M. A.; Peng, C. Y.; Nanayakkara, A.; Challacombe, M.; Gill, P. M. W.; Johnson, B.; Chen, W.; Wong, M. W.; Andres, J. L.; Gonzalez, C.; Head-Gordon, M.; Replogle, E. S.; Pople, J. A. *Gaussian 98*; Gaussian, Inc.: Pittsburgh, PA, 1998.

(23) DALTON, a molecular electronic structure program, Release 2.0 (2005), http://www.kjemi.uio.no/software/dalton/dalton.html.

(24) Zhurko, G. A.; Zhurko, D. A. ChemCraft: Tool for treatment of chemical data, Lite version build 08 (freeware), 2005.

(25) Backe, D. *J. Chem. Phys*. **1993**, *98*, 5648.

(26) Lee, C.; Yang, W.; Parr, R. G. *Phys. Rev*. **1988**, *B37*, 785.

(27) Peng, C.; Ayala, P. Y.; Schlegel, H. B.; Frisch, M. J. *J. Comput. Chem*. **1996**, *17*, 49.

(28) Scott, A. P.; Radom, L. *J. Phys. Chem*. **1996**, *100*, 16502.

(29) Donohue, J.; Trueblood, K. *Acta Crystallogr*. **1956**, *9*, 960.

(30) Roeges, N. P. G. *A Guide to the Complete Interpretation of Infrared Spectra of Organic Structures*; Wiley: New York, 1993.

(31) Jensen, L.; Th. van Duijnen, P. *J. Chem. Phys.* **2005**, *123*, 074.

(32) Kimura, T.; Duan, X.-M.; Kato, M.; Matsuda, H.; Fukuda, T.; Yamada, S.; Okad, S.; Nakanishi, H. *Macromolec. Chem. Phys*. **1998**, *199*, 1193.

(33) Acebal, P.; Blaya, S.; Carretero, L. *J. Phys. B: At. Mol. Opt. Phys.* **2003**, *36*, 2445.

(34) Crystallographic data for the structural analysis have also been deposited with the Cambridge Crystallographic Data Centre, CCDC 628810. Copies of this information may be obtained from the Director, CCDC, 12 Union Road, Cambridge, CB2 1EZ, UK (fax, +44 1223 336 033; e-mail, deposit@ccdc.cam.ac.uk or http://www.ccdc.cam.ac.uk).